Journal of Statistical Physics, Vol. 80, Nos. 3/4, 1995

On the Solutions of the Hypernetted Chain Equation Inside the Gas–Liquid Coexistence Region

Enrique Lomba[1] **and José Luis López-Martín**[1]

Received November 7, 1994

We present a detailed study of the solutions of the hypernetted chain integral equation inside the gas–liquid coexistence region for simple Lennard-Jones fluids. The study is performed by means of a hybrid Newton–Raphson algorithm extended to cope with complex solutions. In this way, we have unequivocally confirmed that the origin of the well-known HNC singular behavior inside the coexistence curve is linked to the onset of complex solutions. As density is increased starting from the vapor phase along isotherms inside the coexistence region, another singularity is encountered (very likely linked with the existence of a complex multiple solution point), and correlations start to diverge. Therefore, with the numerical approach here presented it is not feasible to join the liquid and vapor phases through an analytically continuous path of real and complex solutions. Finally, a study of the transition from the mean spherical approximation behavior (characterized by the presence of a spinodal divergence) to the peculiar hypernetted chain sort of singularity is also presented.

KEY WORDS: Hypernetted chain; integral equations; gas–liquid equilibrium; phase transitions.

1. INTRODUCTION

It has long been known that the hypernetted chain equation (HNC) in systems that undergo phase separation presents a locus of no-solution points which does not coincide with the onset of thermodynamic instability.[1–4] This feature has also been characterized in the Percus–Yevick approximation (PY) for the adhesive hard-sphere fluid (AHSF)[5] and for the two-Yukawa[6] and Lennard-Jones fluids,[7] though in the PY case the lack of spinodal decomposition is specific to the gas phase.

[1] Instituto de Química Física Rocasolano, CSIC, Serrano 119, E-28006 Madrid, Spain.

0022-4715/95/0800-0825$07.50/0

A very detailed and careful study by Belloni[8] attributed the HNC peculiar singular behavior to the presence of square root branch points (SRBP) on the solution, which can easily be identified in the temperature dependence of the isothermal compressibility. The presence of this sort of singularity has been detected in a wide variety of systems, ranging from the Heisenberg spin fluid[9] to, and very specially, the restricted primitive model (RPM) of electrolytes.[10] In this latter case the no-solution line is situated well outside the Monte Carlo prediction of the gas–liquid coexistence curve.[11]

It is then well established that the solution of the HNC equation has singular behavior that has seriously nonphysical features at and near the boundary of a "no-solution" region—a region that appears to signal the presence of phase coexistence. At first glance, it may appear to be a waste of time to pursue a detailed study of such features, since they are artifacts of the approximation. However, because the HNC continues to be such a widely used approximation (because it yields valuable information over large regions of thermodynamic space away from this locus) it seems to us of great interest to understand the precise relationship between the features that are physical and those that are nonphysical in and near this no-solution region. This paper aims to increase that understanding. In this connection, in order to attain a complete picture of the map of solutions of the HNC equation, the integral equation has to be solved in the complex plane, a problem that has been scarcely dealt with in the literature. We are only aware of a few attempts to solve numerically Ornstein–Zernike (OZ)-type integral equations in the complex plane. Cummings and Monson[12] investigated the real and complex solutions of the mean spherical approximations (MSA) for the attractive hard-core Yukawa fluid (HCYF) both analytically and numerically. The same authors developed an extension of Gillan's algorithm[13] to complex variables and studied the different types of solutions of the MSA and PY approximations for HCYF and adhesive hard-sphere (AHSF) fluids.[14] The same systems were also studied by means of a numerical procedure inspired by Baxter's factorization technique, which can appropriately handle nondecaying pair correlation functions.[15] In a different context Strndl and Kahl[16] also developed a complex Gillan algorithm, this time to solve a complex single superchain/effective medium approximation (SSCA/EMA) closure coupled with the OZ equation, a problem that arises when dealing with the electronic density of states or frequency spectrum in disordered media. Even though these mathematical problems are closely related (solving complex OZ equation), the physical nature of the complex solutions of interest is completely different. In our case the complex solution is intrinsic to a problem characterized by real interactions, density, and temperature. In the context of

electronic densities-of-states (or frequency spectra) calculations in disordered media, the complex nature of the solutions comes into existence through complex effective densities which are the result of the mapping of a quantum problem into a classical one.[17]

We thus intend to fill the aforementioned gap, presenting this study of the real (physical and unphysical) and complex solutions of the hypernetted chain equation for one of the most interesting and simple fluid models, the Lennard-Jones system. Inside the complex solution region we have found that by increasing density along an isotherm one finds an additional singularity which seems to be connected to the merging of multiple complex solutions, and marks the onset of diverging pair distribution functions (with long-ranged oscillatory tails). Very likely the outer boundary of this region coincides with the locus of SRBP on the liquid side of the phase diagram. An interesting question that also deserves to be scrutinized concerns the transition from the well-behaved MSA integral equation, always endowed with a spinodal divergence[5, 12] that hides the no-solution region, to the SRBP singularity that marks the onset of complex solutions in the HNC equation. In order to illustrate this transition, we here present an analysis of the low-density, low-temperature solutions of the hybrid mean spherical approximation (HMSA),[18] relaxing the thermodynamic consistency condition, for mixing parameters ranging from a plain HNC closure to a pure soft MSA (SMSA).

The rest of the paper can be sketched as follows: the next section is devoted to a brief explanation of the technicalities required to deal efficiently with a hybrid Newton–Raphson algorithm on the complex plane. In Section 3 we present a detailed examination of the HNC solutions in the two-phase region focusing mainly on the inverse isothermal compressibility and the behavior of the correlation functions. Finally, a comparison with the well-established results of the MSA for the attractive HCYF system is introduced in Section 4, followed by the analysis of the transition from MSA-type to HNC-type singularities.

2. SOLVING THE OZ EQUATION IN THE COMPLEX PLANE

The algorithm for solving the OZ equation that we have generalized to allow for complex solutions is the hybrid Newton–Raphson proposed algorithm by Labík, Malijevsky, and Vonka (LMV).[19] The generalization to complex functions in principle does not pose special difficulties and we have relied on standard computer complex arithmetic and standard mathematical libraries (see IMSL routine DLINCG for an efficient procedure for the inversion of general complex matrices). However, we have found that convergence when approaching the singular points (SRBP) is very slow,

and it becomes extremely difficult, if not impossible, to enter the complex region using as initial estimate a lower-density real solution, even if the change in density is almost negligible. To overcome this difficulty we have devised an approach that has turned out to be extremely powerful in dealing with SRBP singularities. We have perturbed the OZ equation by adding a small imaginary parameter $i\varepsilon$ so that when written in Fourier space the equation reads

$$\tilde{\Gamma} = \frac{\rho \tilde{C}(k)^2}{k - \rho \tilde{C}(k) + i\varepsilon} \tag{2.1}$$

where the tilde denotes a Fourier transformation, and $\tilde{\Gamma}(k) = k(\tilde{h}(k) - \tilde{c}(k))$, $\tilde{C}(k) = k\tilde{c}(k)$ [$h(r)$ and $c(r)$ being the total and direct correlation functions]. Similar definitions hold for the r-dependent functions. The closure relation stays the same, and in the HNC approximation is

$$C(r) = r \exp[-\beta u(r) + \Gamma(r)/r] - \Gamma(r) - r \tag{2.2}$$

The expressions needed to apply to the LMV technique are identical to those proposed by Labík *et al.*,[19] but the Jacobian matrix has to be modified to account for the imaginary perturbing term, i.e.,

$$J_{j,k} = \delta_{ik} - \frac{\rho \tilde{C}_j}{k_j - \rho \tilde{C}_j + i\varepsilon} \left(2 + \frac{\rho \tilde{C}_j}{k_j - \rho \tilde{C}_j + i\varepsilon} \right) \tilde{C}_{j,k} \tag{2.3}$$

and $\tilde{C}_{j,k}$ given by Eq. (13) of ref. 19. The effect of introducing this perturbing parameter can be assessed in Fig. 1, where we have plotted the evolution of the isothermal compressibility along an isotherm in the vicinity of the SRBP singularity, calculated using several ε values ranging from 10^{-1} to 10^{-6}. One sees that the SRBP gives rise to a rapid growth of the imaginary component of the isothermal compressibility (and hence of the imaginary component of the correlation functions). This sudden change affects the stability of the Newton–Raphson procedure, so that if $\varepsilon = 0$, it is not possible to go from real to complex solutions, even if the density is increased by infinitesimal amounts. However, adding a small perturbing imaginary constant to the OZ equation has the effect of smoothing the transition, and in this way the complex solution becomes accessible to the numerical procedure without special difficulties. In order to recover the "true" OZ equation solution, one simply then sets ε to zero, which actually has a very small effect on the solution, except in a tiny area around the singularity. Note that the use of this perturbing imaginary term also removes the real poles from the OZ equation and thus one can safely use this numerical solution procedure across the infinite singularities, as long as

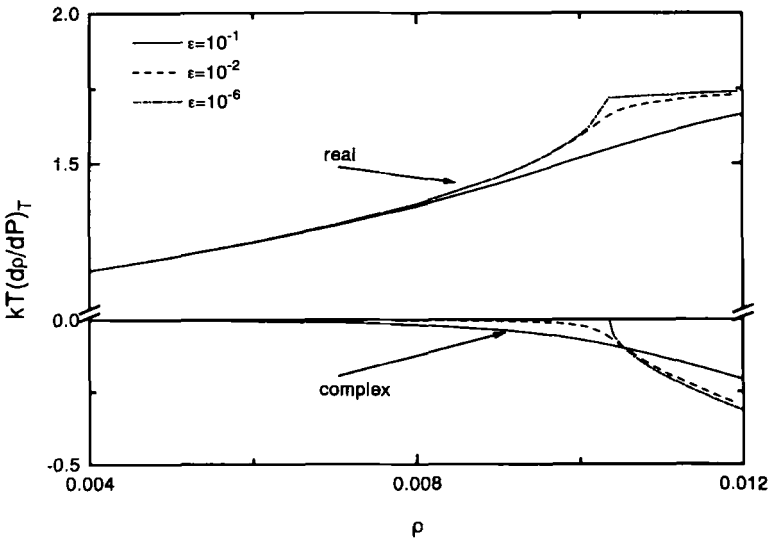

Fig. 1. Real and imaginary components of the HNC isothermal compressibility of a LJ fluid in the vicinity of the SRBP singularity. Dependence on the perturbing imaginary ε parameter [see Eq. (2.1)].

the proper $\varepsilon \to 0$ limit is taken once the singularity has been bypassed, and provided a sufficiently large integration range is chosen.

Once inside the complex region, by stepwise lowering of the density, the real solution is eventually recovered, but we have found that our procedure ends up at the unphysical branch in all cases. This peculiar behavior may be taken profit of in order to generate the set of unphysical real solutions, which according to Belloni are somewhat hard to produce when starting from the physical low-density real branch.[8]

3. THE COMPLEX SOLUTIONS REGION

In the previous section we presented the numerical scheme needed to investigate the behavior of the integral equation inside the two-phase region. The quantity of interest to be monitored is the inverse isothermal compressibility

$$\beta\left(\frac{\partial P}{\partial \rho}\right)_T = 1 - \rho\tilde{c}(0) \tag{3.1}$$

a quantity that vanishes at the spinodal decomposition curve. We have focused on the ρ dependence of this quantity along several isotherms, as

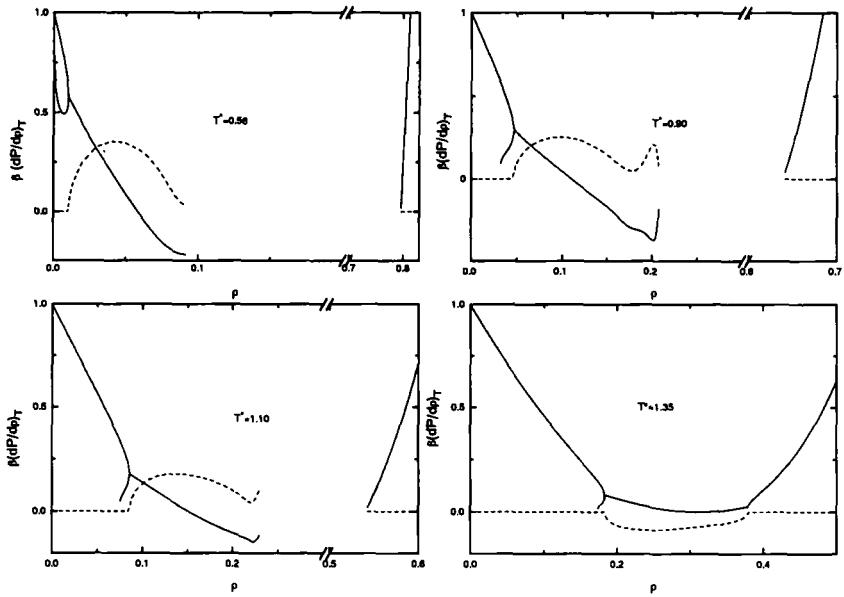

Fig. 2. Inverse isothermal compressibility for a LJ fluid along several subcritical isotherms. Real (solid curves) and imaginary (dashed curves) components.

can be seen in Fig. 2, where we have plotted both its real and imaginary components. Note that, as expected, the onset of complex solutions corresponds to a double solution point, the SRBP. We see that for $T^* = 0.56$ one finds a complete loop formed by the locus of real physical solutions (upper branch) and real unphysical solutions (lower branch). These two branches meet at the SRBP, as was first found by Belloni,[8] and then the solution continues in the complex plane. Also in accordance with the findings of Belloni, at higher T^* the loop unties and several double solution points show up (of which we have only plotted the closest to the HNC termination point). This untying of the loop as T^* increases is needed if the inverse compressibility curve is to evolve smoothly from the convex subcritical curves to the characteristic concave upper-critical curves.

From Fig. 2 there is no doubt that the low-density behavior has little in common with the spinodal divergence. When density increases one finds an additional singularity, which we have analyzed in detail only for $T^* = 1.1$. The isothermal compressibility along this isotherm is represented in the complex region in Fig. 3. This figure shows the dependence of the quantity on the number of integration points used in the numerical procedure, or, more properly, on the integration range. As a matter of fact we

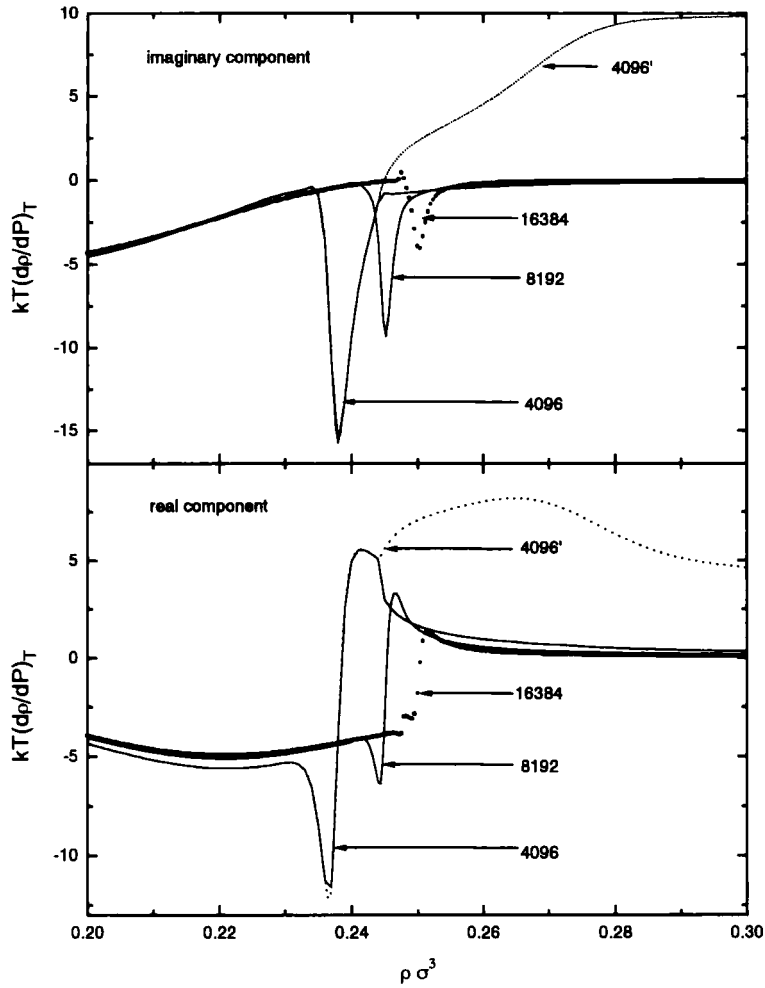

Fig. 3. Dependence of the isothermal compressibility of the integration range inside the complex region. The singular region (onset of diverging correlations) shrinks as the range is increased. Curves are labeled with the number of grid points used in the calculation. The primed label corresponds to a double independent solution obtained.

have found that 8192 grid points and a grid size 0.05σ lead to the same results as 16,384 points and a grid size 0.025σ. The results finally converge for 16,384 grid points, showing no further integration range dependence, at least up to the singularity. As the integration range is increased, the extent of the singularity shrinks, but the numerical procedure becomes more

unstable. Only using 4096 grid points, our numerical procedure could reproduce a second family of solutions, merging close to the singularity, but we believe that for larger integration ranges the multiple solutions must still be present. The merging of complex solutions is very likely the cause of the numerical instability we have encountered when solving the equation in this region.

When crossing the singularity the correlations become extremely long-ranged with clear long-wavelength oscillatory tails, and the numerical procedure becomes unstable. An analysis of the functions in k space shows that the long-ranged oscillations stem from the presence of a singular point in k which is almost a real pole of Eq. (2.1) (with $\varepsilon = 0$). One finds that on the right side of the singularity for a given k_0, $\mathrm{Re}\{1 - \rho\tilde{c}(k_0)\} = 0$ with $\mathrm{Im}\{\rho\tilde{c}(k_0)\}$ being very small. As a matter of fact both quantities change sign in the neighborhood of k_0, but using a discretized algorithm, is not possible to assess whether k_0 is a "true" pole, but the effect on the correlation functions is what one would expect from the presence of a pole for finite-k, long-range oscillatory behavior with a wavelength k_0. Notice that Root and Lovett reported the existence of long-ranged oscillatory real correlations in solution of a one-dimensional YBG equation.[20] Yet, our correlation functions decay more rapidly than $\cos(k_0 r)/r$, since the singularity is not a proper pole, but this might be a numerical artifact. In any case, if one proceeds further to higher densities, the divergence becomes more dominant, and the numerical results become meaningless. A similar phenomenon was described by Monson and Cummings in the PY solutions of the AHS fluid.[14] The authors noticed that at intermediate densities the numerical and analytical results did not agree inside the complex region, which was easily explainable since the analytical results indicated that $h(r)$ became progressively divergent inside that region. This suggest that a Baxter-type method as presented in ref. 15 might be an alternative to bypass this difficulty. The application of these types of numerical methods to the HNC integral equation is, however, somewhat problematic, since this approximation does not fulfill $c(r) = 0$ for $r = R_c$, with R_c a reasonable cutoff distance (like the interaction cutoff), a desirable feature for an easy implementation of the original Baxter formulation.

There are a few observations to be made concerning the ρ dependence of the isothermal compressibility. First, one notices that the region of diverging $h(r)$ shrinks as the temperature increases. Accordingly, the isotherm $T^* = 1.35$, even though still crossing the nonsolution region, lacks any singularity. As T^* is lowered, the high-density SRBP takes the appearance of a spinodal divergence, as mentioned before (see also ref. 10, and obtaining the complex solutions which start at this singularity is not feasible, since correlations diverge in this portion of the complex solution

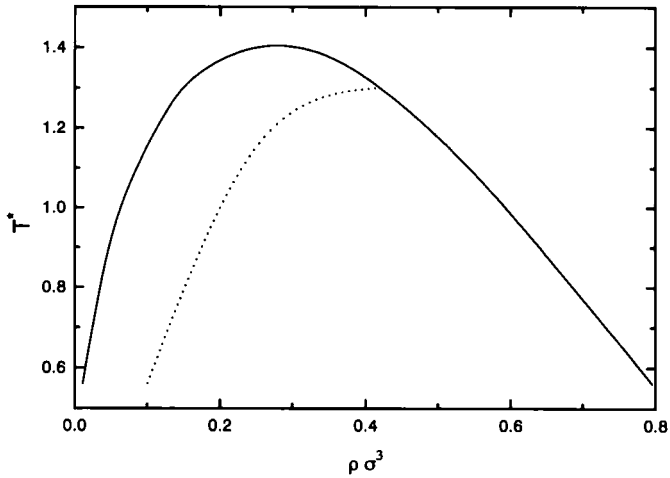

Fig. 4. Complex-solutions boundary of the HNC (solid line). The dotted line represents a portion of the locus of singularities inside the complex regions that marks the onset of diverging pair distribution functions.

region. In Fig. 4 we have represented the boundary of complex solutions together with the locus of complex singularities. One might speculate whether this latter curve might have some connection with a hypothetical spinodal line hidden inside the complex solution region. Such a spinodal line inside the complex region can be determined in the analytical solution of the AHSF in the PY approximation,[5] but it is inaccessible to the type of numerical procedure we use here. There is another aspect to be mentioned, and it concerns the two types of real solutions of the integral equation at subcritical T^* close to the SRBP singularities. The existence of physical and unphysical solutions in the vicinity of these sorts of singularities was first pointed out by Belloni[8] for the HCYF in the HNC approximation. In this case it was found that both solutions are perfectly compatible with the integral equation, and *are not artifacts* of the numerical procedure. Both correlation functions decay to zero and there is nothing to object to in any of them, except that the unphysical solution yields an isothermal compressibility that decreases with density along the subcritical isotherm in the gas phase, a behavior improper of a vapor. In this connection, we have found that the same features hold for the LJ fluid. In Fig. 5 we illustrate the physical and unphysical correlation functions for a state close to the SRBP. Very likely, if analyzed in the framework of the treatment of Schlijper and co-workers,[2–4] one would find that the unphysical solution does not correspond to a minimum of the HNC free

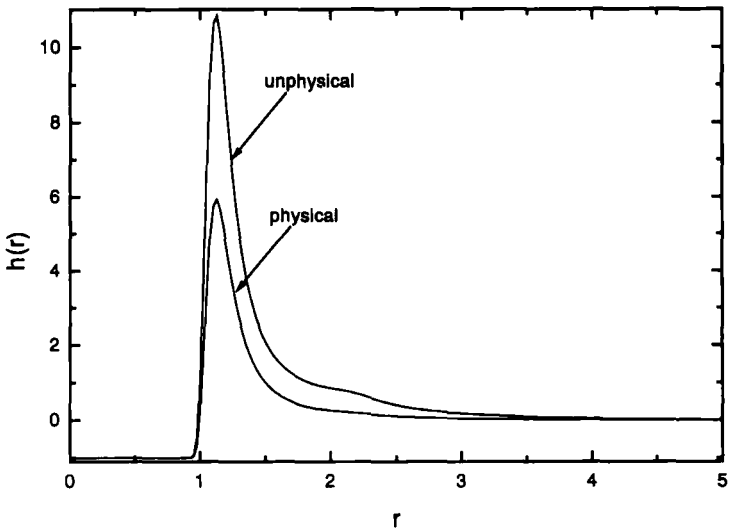

Fig. 5. Total correlation function for the physical and unphysical solutions of the HNC equation in the LJ fluid at $T^* = 0.56$ and $\rho^* = 0.008$.

energy functional, but to a local maximum or saddle point; this, though consistent with the fact that the termination points of the HNC (SRBP) are saddle points of the free energy surface,[3,4] has not been proven. Unfortunately, the hybrid Newton–Raphson method we use does not provide information on the complete Jacobian matrix of the integral equation, and therefore the elegant analysis of the free energy Hessian presented in ref. 4 is beyond our reach at present. We have met here an essential difference with respect to the MSA solution of the HCYF. In this case the inverse isothermal compressibility also exhibits a similar loop, but with the double solution point at densities higher than the spinodal (see next section). The solutions on the unphysical branch correspond now to diverging pair distribution functions.[12] By contrast, in our case the only difference between the physical and unphysical correlation functions is the much higher first peak and presence of a shoulder around the second coordination shell in the unphysical solution. Both correlation functions indicate a large amount of clustering around the particle at the origin.

For the sake of completeness, in Fig. 6 we present the real and imaginary components of the total correlation function $h(r)$ for several densities close to the boundary. The physical meaning of these functions, if any, is not easy to grasp. Both components have the appearance of well-behaved correlation functions with large values in the first coordination

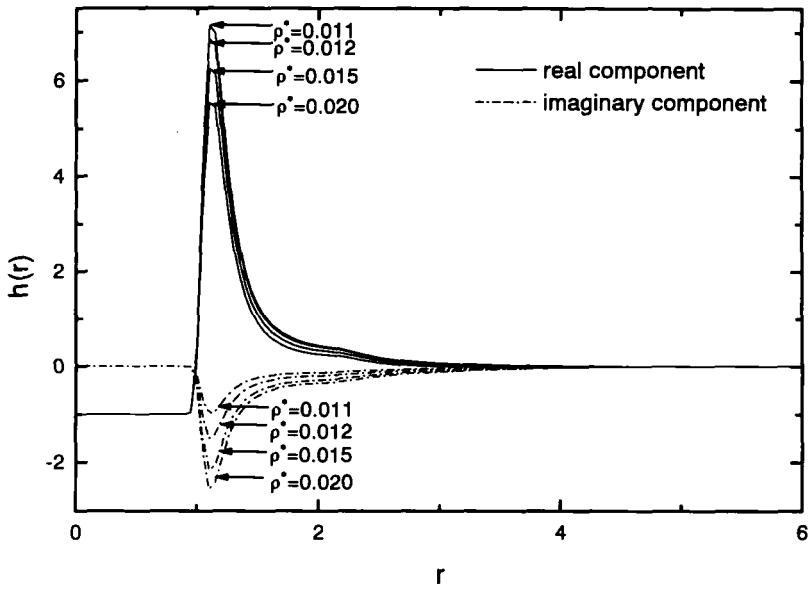

Fig. 6. Real and imaginary components of the total correlation function for the LJ fluid at $T^* = 0.56$ in the vicinity of the boundary.

shell, and little else can be inferred from them. We see that in the neighborhood of the SRBP, small increments in density are associated with a rapid growth of the imaginary component of the correlation functions. This is the main reason for the lack of stability of numerical solutions in this region.

Finally, at this stage, we ought to mention that the results here presented were obtained using 8192 mesh points and a grid size $\Delta r = 0.025\sigma$. Several calculations were carried out with 16,834 points and/or grid size 0.05σ to guarantee the accuracy of the results.

4. HNC VS. MSA-LIKE BEHAVIOR

In the previous section we already mentioned that there are some substantial differences in the behavior of the HNC and MSA integral equations when approaching the two-phase boundary. To illustate more clearly these differences, in Fig. 7 we show the ρ dependence of the inverse isothermal compessibility of the HCYF in the MSA, both in complex and in real space. In contrast with our observations on the HNC approximation, here this quantity vanishes approaching the axis with zero slope, and as a result the physical branch has opposite convexity when compared with the HNC result. One then enters a region of diverging $h(r)$ which ends at a double

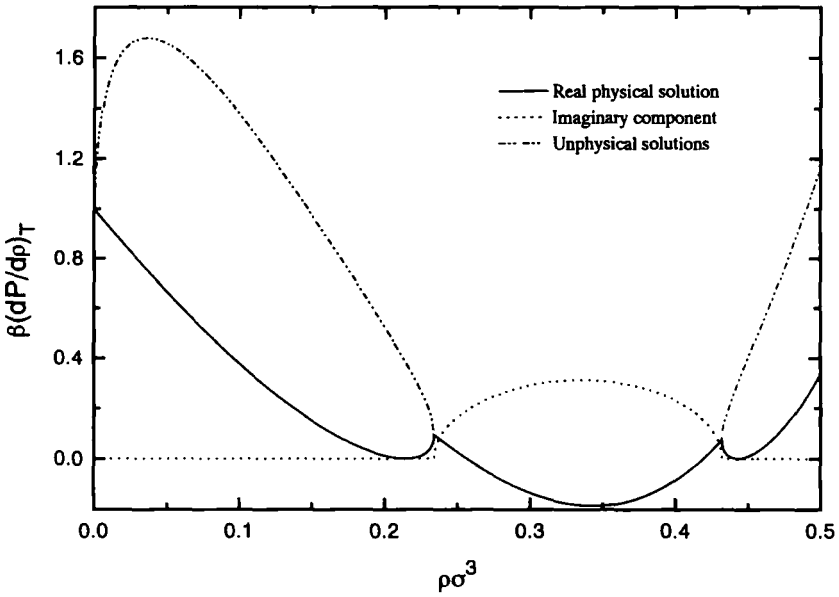

Fig. 7. Inverse isothermal compressibility of the attractive HCYF in the MSA approximation.

solution point, where the physical (lower) and unphysical (upper) branches meet. The relative position of physical and unphysical branches in the HNC is inverted, as can be seen in Fig. 2. In the MSA, for higher densities the solution enters in the complex region, which ends at another double solution point, and then the high-density spinodal is encountered, thus forming a rather symmetric plot.

It is possible to have a more clear picture of the transition between MSA-like and HNC-like behavior by resorting to the HMSA closure, namely

$$g(r) = \{\exp[-\beta u_1(r)]\}\left[1 + \frac{\exp\{f(r)[-\beta u_2(r) + h(r) - c(r)]\} - 1}{f(r)}\right] \quad (4.1)$$

where u_1 and u_2 are the repulsive and attractive components of the potential split according to the Weeks–Chandler–Andersen prescription[18] and $f(r) = 1 - \exp(-\alpha r)$ is the mixing function. Contrary to the proper HMSA formulation, we will not require here thermodynamic consistency to determine the value of α. Moreover, in the gas phase, which is the one we are now more interested in, thermodynamic consistency forces the HMSA to behave more and more HNC-like as the density is lowered.[18] We have

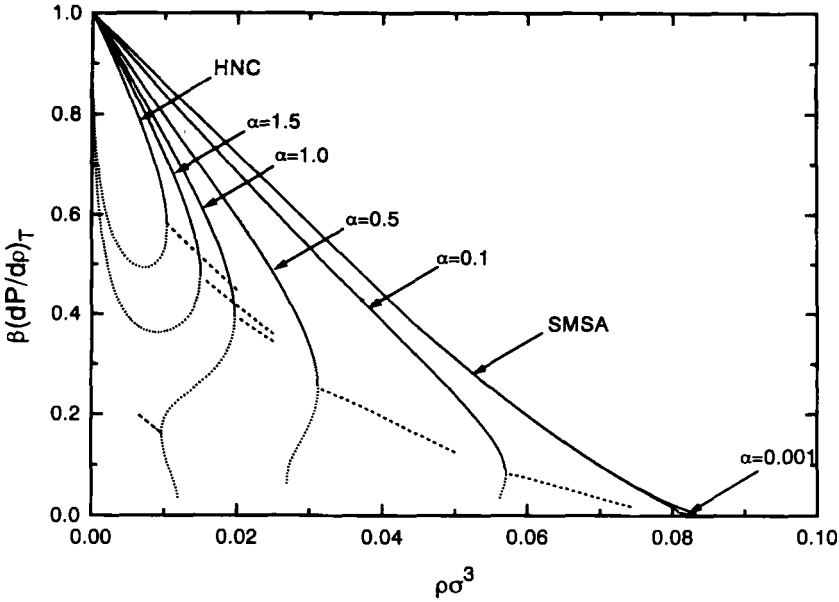

Fig. 8. Inverse compressibility for various HMSA-type approximations [see Eq. (4.1)]. Solid curves denote physical branches, dotted curves unphysical branches, and dashed lines correspond to the real component of the complex solution. The calculations correspond to the $T^* = 0.56$ isotherm.

studied the isotherm $T^* = 0.56$ for a variety of α values, ranging from the SMSA ($\alpha = 0$) to the HNC ($\alpha = \infty$). The evolution of the inverse compressibility for the different closures considered is summarized in Fig. 8. Together with the physical and unphysical branches of real solutions, a portion of the real component of the complex solution has been included as well. From Fig. 8 one can readily see how increasing the MSA component breaks the original HNC loop, by which one then finds several double solution points, from which the complex solutions can be accessed. Only a limited number of these points have been shown on the plot, and solely for $\alpha = 1$, since proceeding further becomes computationally more cumbersome as the correlation functions turn into slowly decaying functions and the integration range has to be increased. As the MSA component is augmented (the value of α is lowered), the complex region comes into existence at higher densities and the value of the inverse isothermal compressibility at the endpoint is smaller, until the SMSA curve is reached. This curve ends up at $\beta(dP/d\rho) = 0$, that is, at the spinodal line and with zero slope, precisely the well-known behavior of the analytic MSA solution for the attractive HCYF (see Fig. 7). We have been unable to continue the SMSA

solution for higher densities, probably due to the fact that our solution method is inappropriate to handle diverging $h(r)$ functions. Nonetheless, Fig. 8 explains how the transition from HNC to MSA can be smoothly accomplished, and why physical and unphysical branches exchange positions when going from one approximation to the other. Notice that a similar untying of the HNC loop occurs when the temperature is raised (see Fig. 2) and is also due to the continuity of the transition between curves of opposite convexity (supercritical vs. subcritical and MSA vs. HNC).

We have presented a detailed analysis of the HNC approximation behavior at subcritical temperatures, with emphasis on the low-density (vapor-phase) behavior. We have shown unequivocally that the peculiarities of the HNC behavior in the vicinity of the coexistence curve stem from the onset of complex solutions. This does not preclude, but complements other explanations which connect the singularity with the loss of local convexity of the HNC free energy.[2–4] At very low densities, where the HNC is nearly an exact theory, it is clear that the bridge function (though it vanishes quadratically with density) must play a "fine-tuning" role that should shift the complex solution boundary into the limits of the spinodal line. The recently proposed INV integral equation[21] for the RPM of electrolytes has been shown to have the boundary of the nonsolution line at considerably lower temperatures than those reached by the HNC (which are known to be well off the simulated values).[22] The properties of this and related closures might give some clue to future improvements of integral equation theories in the vicinity of the two-phase region.

ACKNOWLEDGMENTS

The authors would like to thank Prof. G. Stell and Prof. L. L. Lee for their critical reading of the manuscript and their helpful suggestions. Fruitful correspondence with Dr. P. A. Monson and Prof. M. M. Telo da Gama is also acknowledged. This work has been financed by the Spanish Dirección General de Investigación Científica y Técnica (DGICYT) under grant no. PB91-0110.

REFERENCES

1. E. Lomba, in *Supercritical Fluids. Fundamentals for Application*, E. Kiran and J. M. H. Levelt-Sengers, eds. (Kluwer, Dordrecht, 1994).
2. A. G. Schlijper, M. M. Telo da Gamma, and P. G. Ferreira, *J. Chem. Phys.* **98**:1534 (1993).
3. P. G. Ferreira, R. L. Carvalho, M. M. Telo da Gama, and A. G. Schlijper, *J. Chem. Phys.* **101**:594 (1994).

4. A. G. Schlijper, L. E. Scales, J. E. Rycroft, M. M. Telo da Gama, and P. G. Ferreira, *Int. J. Thermophys.*, to be published.
5. P. T. Cummings and G. Stell, *J. Chem. Phys.* **78**:1917 (1983).
6. F. Gallerani, G. Lo Vecchio, and L. Reatto, *Phys. Rev. A* **32**:2526 (1985).
7. F. Gallerani, G. Lo Vecchio, and L. Reatto, *Phys. Rev. A* **31**:511 (1985); B. C. Freasier and R. J. Bearman, *J. Chem. Phys.* **100**:3094 (1994).
8. L. Belloni, *J. Chem. Phys.* **98**:8080 (1993).
9. E. Lomba, J. J. Weis, N. G. Almarza, F. Bresme, and G. Stell, *Phys. Rev. E* **49**:5169 (1994).
10. J. S. Høye, E. Lomba, and G. Stell, *Mol. Phys.* **79**:523 (1993).
11. J. M. Caillol, *J. Chem. Phys.* **100**:2161 (1994).
12. P. T. Cummings and P. A. Monson, *J. Chem. Phys.* **82**:4303 (1985).
13. M. J. Gillan, *Mol. Phys.* **38**:1781 (1979).
14. P. A. Monson and P. T. Cummings, *Int. J. Thermophys.* **6**:573 (1985).
15. P. T. Cummings and P. A. Monson, *Int. J. Thermophys.* **11**:97 (1990).
16. C. F. Strndl and G. Kahl, *J. Phys.: Condens. Matter.* **5**:6801 (1993).
17. D. E. Logan and M. D. Winn, *J. Phys. C* **21**:5773 (1988); B. C. Xu and R. M. Stratt, *J. Chem. Phys.* 5613 (1989).
18. G. Zerah and J. P. Hansen, *J. Chem. Phys.* **84**:2336 (1986).
19. S. Labík, A. Malijevsky, and P. Vonka, *Mol. Phys.* **56**:709 (1985).
20. L. J. Root and R. Lovett, *J. Chem. Phys.* **95**:8390 (1991).
21. D. M. Duh and A. D. J. Haymet, *J. Chem. Phys.* **97**:7716 (1992).
22. F. Bresme, E. Lomba, J. J. Weis, and J. L. F. Abascal, *Phys. Rev. E* **51**:289 (1995).